⌘ *Author's Choice*

THE JOURNAL OF BIOLOGICAL CHEMISTRY VOL. 284, NO. 15, pp. 10076–10087, April 10, 2009

Crystal Structure of Malaria Parasite Nucleosome Assembly Protein

DISTINCT MODES OF PROTEIN LOCALIZATION AND HISTONE RECOGNITION[*][S]

Received for publication, November 13, 2008, and in revised form, January 9, 2009 Published, JBC Papers in Press, January 27, 2009, DOI 10.1074/jbc.M808633200

Jasmita Gill[‡1], Manickam Yogavel[‡1], Anuj Kumar[‡2], Hassan Belrhali[§], S. K. Jain[¶], Melanie Rug[‖], Monica Brown[‖], Alexander G. Maier[‖3], and Amit Sharma[‡4]

From the [‡]Structural and Computational Biology Group, International Centre for Genetic Engineering and Biotechnology, Aruna Asaf Ali Road, New Delhi 110067, India, the [§]European Molecular Biology Laboratory, 6 Rue Jules Horowitz, BP 181, F-38042 Grenoble Cédex 9, France, the [¶]Department of Biotechnology, Hamdard University, Hamdard Nagar, New Delhi 110062, India, and the [‖]Walter and Eliza Hall Institute of Medical Research, 1G Royal Parade, Parkville, Victoria 3050, Australia

Nucleosome assembly proteins (NAPs) are histone chaperones that are essential for the transfer and incorporation of histones into nucleosomes. NAPs participate in assembly and disassembly of nucleosomes and in chromatin structure organization. Human malaria parasite *Plasmodium falciparum* contains two nucleosome assembly proteins termed PfNapL and PfNapS. To gain structural insights into the mechanism of NAPs, we have determined and analyzed the crystal structure of PfNapL at 2.3 Å resolution. PfNapL, an ortholog of eukaryotic NAPs, is dimeric in nature and adopts a characteristic fold seen previously for yeast NAP-1 and Vps75 and for human SET/TAF-1b (β)/INHAT. The PfNapL monomer is comprised of domain I, containing a dimerization α-helix, and a domain II, composed of α-helices and a β-subdomain. Structural comparisons reveal that the "accessory domain," which is inserted between the domain I and domain II in yeast NAP-1 and other eukaryotic NAPs, is surprisingly absent in PfNapL. Expression of green fluorescent protein-tagged PfNapL confirmed its exclusive localization to the parasite cytoplasm. Attempts to disrupt the PfNapL gene were not successful, indicating its essential role for the malaria parasite. A detailed analysis of PfNapL structure suggests unique histone binding properties. The crucial structural differences observed between parasite and yeast NAPs shed light on possible new modes of histone recognition by nucleosome assembly proteins.

Chromatin assembly and remodeling are vital cellular processes that are pivotal during replication, transcription, recombination, and repair in eukaryotic cells. Nucleosomes are the fundamental repeating subunits of all eukaryotic chromatin (except when packaged in sperm). Nucleosomes are made up of DNA and four pairs of histone proteins, which together resemble "beads on a string" when observed with an electron microscope. Histones H2A, H2B, H3, and H4 are part of the nucleosome, whereas histone H1 sits on top of the structure, keeping in place the DNA that is wrapped around the other histones (1). Nucleosome assembly is a fundamental biological process that is required for the replication and maintenance of chromatin in the eukaryotic nucleus. In dividing cells, newly synthesized DNA is assembled rapidly into chromatin by a process that appears to involve an indirect coupling between DNA replication and nucleosome assembly. The assembly of nucleosome occurs in a two-step process: a tetramer of H3 and H4 is first deposited onto DNA, and then the nucleosome core is completed by the addition of two heterodimers of H2A and H2B (1, 2). Histones are highly basic proteins and require chaperones that promote their proper interaction to form chromatin. Histone chaperones also prevent nonspecific aggregation of DNA with histones. A number of histone chaperones (*e.g.* nucleosome assembly protein 1 (NAP-1),[5] nucleoplasmin, Asf1 (antisilencing function), CAF-1 (chromatin assembly factor), and HirA (histone regulator A)) are involved in nucleosome/chromatin assembly/disassembly (3).

Some histone chaperones, such as nucleoplasmin and NAP-1, exhibit a preference for binding to histones H2A and H2B relative to histones H3 and H4 (4, 5). Other histone chaperones, which include CAF-1, N1/N2, and Spt6, associate preferentially with H3 and H4. Interestingly, it has also been observed that newly synthesized histones are acetylated (such as at positions 5, 8, and 12 of histone H4) and then subsequently deacetylated after assembly into chromatin (6, 7). Thus, factors that mediate histone acetylation or deacetylation may participate, perhaps indirectly by the covalent modification of his-

* This work was supported in part by a grant from the Department of Biotechnology, Govt. of India. The x-ray facility at the International Centre for Genetic Engineering and Biotechnology, New Delhi, is funded by the Wellcome Trust. The costs of publication of this article were defrayed in part by the payment of page charges. This article must therefore be hereby marked "*advertisement*" in accordance with 18 U.S.C. Section 1734 solely to indicate this fact.

⌘ *Author's Choice*—Final version full access.

The atomic coordinates and structure factors (code 3FS3) have been deposited in the Protein Data Bank, Research Collaboratory for Structural Bioinformatics, Rutgers University, New Brunswick, NJ (http://www.rcsb.org/).

[S] The on-line version of this article (available at http://www.jbc.org) contains supplemental Figs. S1–S6 and Table S1.

[1] Supported by the Wellcome Trust.

[2] Supported by a Department of Biotechnology, Government of India, fellowship.

[3] An Australian Research Council Research Fellow.

[4] An International Wellcome Trust Senior Research Fellow in Biomedical Sciences. To whom correspondence should be addressed. Tel./Fax: 911126741731; E-mail: amit.icgeb@gmail.com.

[5] The abbreviations used are: NAP, nucleosome assembly protein; yNAP-1, yeast NAP-1; hSET, human SET; SAD, single anomalous dispersion; NES, nuclear export signal; DAPI, 4′,6-diamidino-2-phenylindole; GFP, green fluorescent protein; ELISA, enzyme-linked immunosorbent assay; PBS, phosphate-buffered saline; NLS, nuclear localization signal; r.m.s., root mean square.

tones, in the chromatin assembly process. Homologs of yeast NAP-1 are conserved among all eukaryotes, and yeast NAP-1 is well characterized for its role in chromatin assembly (3, 8). Gene knock-out phenotypes in several studied organisms indicate essentiality of the nucleosome assembly protein family; gene ablations in mouse and *Drosophila* cause embryonic lethality, whereas in yeast, cells exhibit growth defects (9–11).

Malaria is one of the most common infectious diseases and remains an enormous public health problem. Malaria is caused by protozoan parasites of the genus *Plasmodium*, and the most serious forms of the disease are caused by *Plasmodium falciparum* (12). It is therefore crucial to identify, dissect, and exploit the molecular motors of malaria parasites, which can serve as essential targets for antimalarials. The human malaria parasite *P. falciparum* contains two nucleosome assembly proteins, which we have termed PfNapL and PfNapS and which are orthologs of eukaryotic NAPs (13). We have shown that both PfNapL and PfNapS are present in all erythrocytic stages of the parasite (13). PfNapL forms complexes with both histone tetramer and octamer and is predominantly localized in the cytoplasm in the asexual and sexual stages of the parasite (13, 14). PfNapL by itself is unable to deposit the histones onto DNA, but it can interact with both core and linker histones and is involved in histone binding, shuttling, and transfer/release, as shown earlier (13, 14) (Fig. 1*f* reproduced here from Ref. 14). The histone binding characteristics of PfNapL have been detailed previously, including its ability to transfer cytoplasmic histones on to PfNapS (which is localized both in cytoplasm and the nucleus and transfers histones into the nucleus for deposition) (14). A model for relay of histones from parasite cytoplasm to the nucleus has also been proposed by us previously (see Ref. 14 and specifically Fig. 1*f*). PfNapL preferentially interacts with the H3-H4 tetramer histones over H2A and H2B histones. PfNapL and PfNapS do not interact with each other (14). To address the structural basis of the nucleosome assembly activity in *P. falciparum*, we have determined and analyzed the crystal structure of PfNapL. Here, we detail the PfNapL structure and compare it with histone chaperones like yeast NAP-1 (yNAP-1), human SET/TAF-1b (β)/INHAT (hSET), Vps75, and Asf1-histone complex (15–21) in order to provide new insights into the mechanism of histone recognition.

EXPERIMENTAL PROCEDURES

Protein Crystallization and Data Collection—PfNapL crystals were obtained at 20 °C by the hanging drop vapor diffusion method using l μl of full-length purified PfNapL protein (13, 14) (3 mg ml^{-1} in buffer containing 25 mM Tris and 25 mM NaCl) and l μl of 0.2 M $MgCl_2$ with 20% polyethylene glycol 3350 (mother liquor). A single crystal was transferred to cryoprotectant containing a higher concentration of mother liquor (30% polyethylene glycol 3350 and 0.3 M $MgCl_2$) supplemented with 0.5 M NaI for 30 s and flash-frozen under a stream of nitrogen gas at 100 K. X-ray diffraction data were collected on an in-house rotating anode MICRO MAX 007 x-ray generator (wavelength of 1.54 Å; Rigaku/MSC) operated at 40 kV and 20 mA with Osmic mirrors (Vari Max HR). The images were recorded using an MAR345dtb imaging plate, and the iodide-single anomalous dispersion (SAD) data set was collected to 3.0 Å resolution. The iodide-soaked crystals of PfNapL belong to the monoclinic space group C2 with cell dimensions of a = 76.68 Å, b = 37.83 Å, c = 79.31 Å, and β = 99.83°, having one monomer per asymmetric unit. High resolution native diffraction data to 2.3 Å resolution were collected at the BM14 beamline (European Synchotron Radiation Facility, Grenoble, France). These crystals also belong to the monoclinic space group C2 with different cell dimensions of a = 92.41 Å, b = 38.12 Å, c = 80.05 Å, and β = 107.87°. The diffraction images were processed and scaled with the HKL2000 suite (22).

Phasing, Structure Determination, Refinement, and Analysis—The structure was determined using the iodide-SAD technique, and phasing was achieved by utilizing four iodide sites to 3.0 Å resolution using PHENIX (23). An initial model was built automatically without side chains and subsequently rebuilt manually using COOT (24). The high resolution structure was determined by molecular replacement technique using the PfNapL iodide-SAD model. This model to 2.3 Å resolution was further refined using CNS (25) (Table 1). The final model was validated using PROCHECK (26). All figures were generated using Chimera (27). The least square fittings and structural alignment were carried out using LSQMAN (28). Electrostatic potential surfaces were generated using GRASP (29).

Parasite Culture, Plasmid Constructs, and Transfection—*P. falciparum* of the 3D7 strain were cultured *in vitro* in O+ human erythrocytes using standard conditions (30). For the gene deletion construct, we amplified the 5′- and 3′-targeting segments of PfNapL using the primer pairs aw775/aw776 and aw777/778, resulting in 645- and 622-bp products, respectively. After amplification, the targeting segments were cloned into the pCC-1 vector (31) using SacII/SpeI for the 5′ and EcoRI/AvrII for the 3′ segment, resulting in the pCC-1ΔPfNapL plasmid. After proliferation of the plasmid DNA in *Escherichia coli* PMC103 cells and purification with a Qiagen Maxi kit, 80 μg of plasmid DNA was taken up in cytomix and transfected via electroporation using standard procedures (32). Parasites containing the plasmid were selected for in the presence of 2 nM WR99210 (33). The resulting parasite population was then subjected to two off/on drug cycles for 21 days each to encourage the loss of free plasmid. After each addition of WR99210, a subpopulation was selected on 231 nM 5-fluorocytosine in the presence of WR99210 (to encourage double recombination events) and analyzed via Southern blot. Two independent rounds of transfections were performed and analyzed: Aw775, atcccgcggTATTTGAATTTGATTTCTTGC; Aw776, gatactagtGCTAGTTAAATAAACATAACAG; Aw777, atcgaattcGTATGCAACTACTTTTTCG; Aw778, gatcctaggCTGTATGTAATAACACTGGCTCG.

To generate transgenic parasites expressing GFP chimeras, we amplified the sequence encoding PfNapL from cDNA and cloned the product into the pARL vector (34) to create PfNapL-pARL. Conserved residues of the putative nuclear export signal (NES) were mutated by yielding the plasmids PfNapL L46A-pARL and PfNapL Q50A-pARL. The expression of chimeric proteins in this vector is driven by the *crt* promoter. The correctness of each construct was confirmed by DNA sequencing. 3D7 *P. falciparum* parasites were transfected with 100 μg of

plasmid DNA (Qiagen) by electroporation and cultured in the presence of 2 nM WR99210 (32).

Microscopy—In order to observe the localization of the GFP chimeras in all three generated cell lines, live cells were stained with DAPI and immediately processed for viewing at ambient temperature. Cells were viewed with an Apochromat ×100/1.4 numerical aperture oil DIC lens on a Zeiss Axioskop 2 microscope equipped with a PCO SensiCam (12-bit) camera and Axiovision 3 software. Captured images were processed using Photoshop and ImageJ software (available on the World Wide Web).

Histone-binding ELISAs—Residues Asp^{192}, His^{227}, Thr^{230}, Glu^{260}, Lys^{266}, Asp^{233}, Tyr^{259}, Ile^{136}, and Ile^{147} were mutated to alanine using the QuikChange site-directed mutagenesis kit (Stratagene). Tetramer and octamer forms of calf thymus histone were reconstituted from individual histones (Roche Applied Science) after denaturing and refolding according to the method developed by Tanaka *et al.* (35). ELISAs were performed by coating individual histones, histone tetramers, or histone octamers (100 ng/well) in microtiter plates (Nunc). The histones were coated on plates in phosphate-buffered saline (PBS) and incubated at 4 °C overnight. The following day, the plates were washed with PBS plus 0.2% Tween 20 (PBST) and blocked with 3% PBS-bovine serum albumin (200 μl/well) and incubated for 1 h at 37 °C. Then 100 μl of purified PfNapL (concentration ranging from 25 to 800 ng) was added to each well in histone-binding buffer (20 mM HEPES, 7.5 mM $MgCl_2$, 1 mM dithiothreitol, 0.5 mM EDTA, and 50 mM KCl, pH 7.5). Plates were incubated for an additional 1 h at 37 °C and washed three times with PBST, and then PfNapL anti-rabbit polyclonal antibodies were added to each well (1:25,000 dilutions). After incubation at 37 °C for 1 h, three more PBST washes were done, followed by the addition of horseradish peroxidase-conjugated secondary antibody (anti-rabbit), and incubated for an additional 1 h at 37 °C. After three more PBST washes, a color reaction was developed using orthophenylenediamine (Sigma) and H_2O_2 in citrate-phosphate buffer. The optical density was measured at 490 nm using an ELISA plate reader (Molecular Probes). Bovine serum albumin, primary antibodies, and secondary antibodies were separately used as controls in these ELISAs.

RESULTS

Structure Determination and Overall Structure of PfNapL—The crystal structure of PfNapL was determined using the iodide-SAD technique at 3.0 Å and refined using high resolution data to 2.3 Å resolution (Table 1). Purified PfNapL crystallized in monoclinic space group C2 with solvent content of 55%, and the asymmetric unit contains one monomer of PfNapL. For a total of 347 residues of full-length PfNapL (molecular mass ~41 kDa), electron density was observed for the central core residues 33–281. The N- and C-terminal regions in PfNapL were presumably cleaved off during protein processing prior to crystallization. The regions 89–91, 138–144, 171–178, 200–221, and 235–246 have weak electron density and are disordered in the overall structure. The final refined model of PfNapL has R_{factor} and R_{free} values of 21.8 and 28.5%, respectively (Table 1).

TABLE 1
Data collection and refinement statistics

Parameter	Native	Iodide-SAD
Data collection		
Cell dimensions	a = 92.41 Å, b = 38.12 Å, c = 80.05 Å, and β = 107.87°	a = 76.68 Å, b = 37.83 Å, c = 79.31 Å, and β = 99.83°
Wavelength (Å)	1.0	1.54
Anomalous scatterer		I
Resolution (Å)	50-2.3	50-3.0
Outer shell resolution (Å)[a]	2.38-2.3	3.11-3.0
No. of unique reflections	12,065 (1217)	4606 (451)
Redundancy	5.1 (5.1)	14.5 (13.2)
R_{merge}[b]	0.052 (0.238)	0.084 (0.331)
Completeness (%)	100 (99.9)	99.0 (97.6)
$I/\sigma I$	26.1 (4.98)	45.6 (11.4)
Phasing (PHENIX)		
AutoSol figure of merit		0.36
Post DM-figure of merit		0.66
Refinement		
Resolution range (Å)	50–2.3	
No. of reflections (test set)	1219	
R_{factor}/R_{free} (%)	21.8/28.5	
No. of protein atoms	1668	
No. of water molecules	74	
***B* factor (Å²)**		
Protein atoms	36.6	
Water atoms	35.1	
Stereochemistry		
r.m.s. deviation bond length (Å)	0.01	
r.m.s. deviation bond angle (degrees)	1.50	
Ramachandran plot		
In most favored regions (%)	91.5	
In additionally allowed regions (%)	7.4	
In generously allowed regions (%)	1.1	

[a] Numbers in parentheses are values in the highest resolution shell.
[b] $R_{merge} = \Sigma|I_{obs} - \langle I\rangle|/\Sigma\langle I\rangle$ summed over all observations and reflections.

The NAP/SET proteins consist of a central region of ~250 residues that are thought to be primarily responsible for histone binding (Fig. 1*a*). In general, NAPs comprise low complexity sequences in their N and C termini, wherein the C terminus usually contains stretches of acidic residues (Fig. 1*a*). The overall fold of PfNapL is similar to yNAP-1 and hSET (15, 16) (Fig. 1*b*). Each monomer contains a domain I composed of a dimerization helix α2 (residues 37–87). The monomer also contains domain II, which is composed of α-helices (α3 (residues 102–108), α4 (residues 111–116), and α5 (residues 119–127)), a β subdomain containing four antiparallel β-strands (residues 128–185), another α-helix α7 (residues 225–228), and a final two α-helices on the other side of the β subdomain (α7 (residues 248–267) and α8 (residues 269–277)) (Fig. 1*b*). We have earlier shown the dimeric nature of PfNapL in solution (13). The crystallographic 2-fold symmetry generates a homodimer of PfNapL of ~87 × 52 × 33 Å with a total buried surface area of 4209 Å². The 51-residue-long dimerization helix α2 forms the characteristic shape of PfNapL, wherein two backbone helices cluster in an antiparallel manner to form the dimer using mainly hydrophobic interactions and few salt bridges/hydrogen bonds (Fig. 1*b*). The overall sequence identity of PfNapL with yNAP-1, hSET, and Vps75 is 24, 25, and 14%, respectively. (15–19) (Fig. 1*c* and Fig. S1). The phylogenetic analysis of NAPs suggests greater evolutionary distance of malaria parasite NAPs from homologs in yeast and humans (available on the World Wide Web) (Fig. 1*e*).

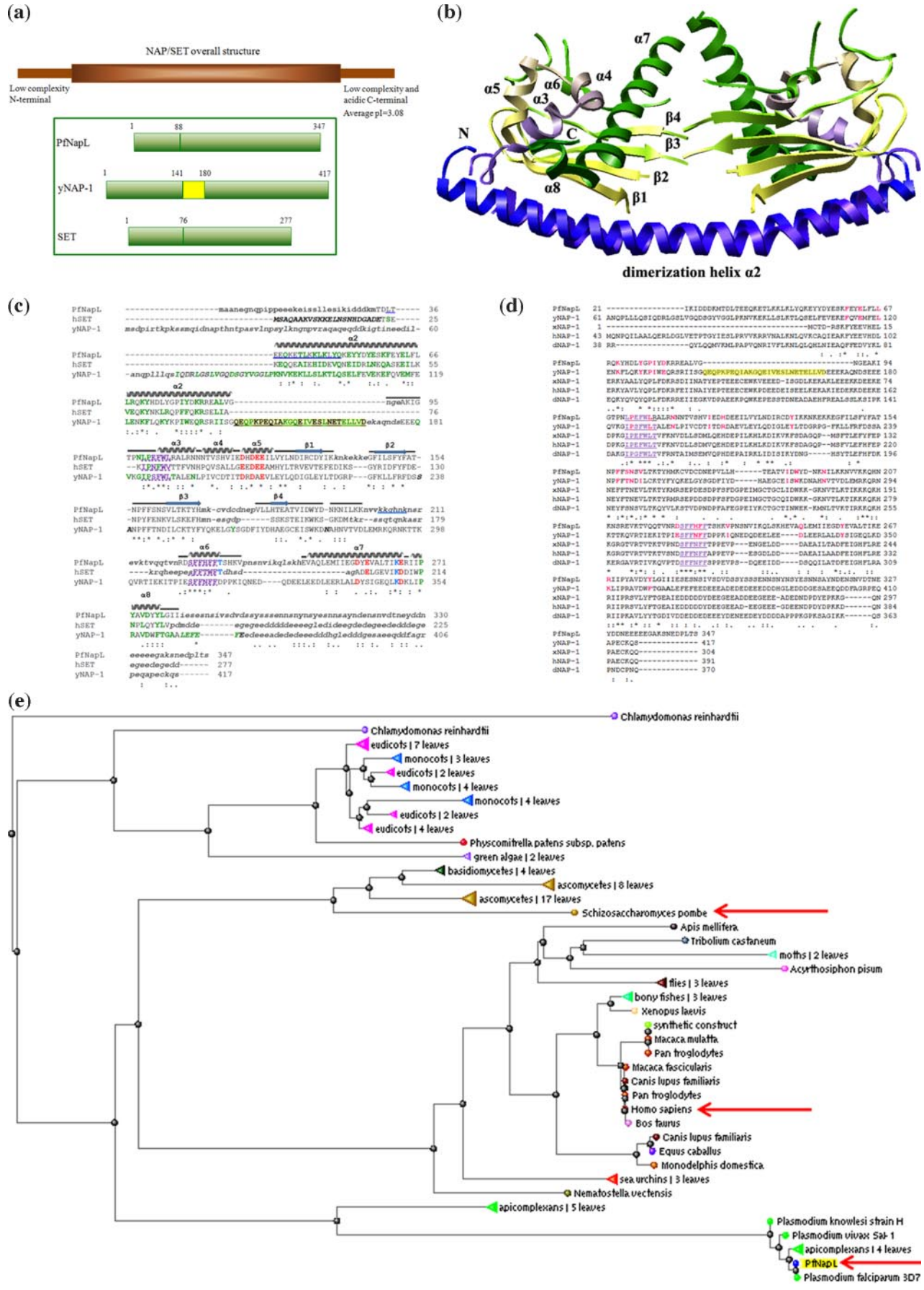
(a)
NAP/SET overall structure
Low complexity
N-terminal
Low complexity and
acidic C-terminal
Average pI=3.08
PfNapL
yNAP-1
SET
(b)
α7
α5
α6
α4
α3
β4
N
C
β3
β2
α8
β1
dimerization helix α2
(c)
(d)
(e)
Chlamydomonas reinhardtii
eudicots | 7 leaves
monocots | 3 leaves
eudicots | 2 leaves
monocots | 4 leaves
monocots | 4 leaves
eudicots | 2 leaves
eudicots | 4 leaves
Physcomitrella patens subsp. patens
green algae | 2 leaves
basidiomycetes | 4 leaves
ascomycetes | 8 leaves
ascomycetes | 17 leaves
Schizosaccharomyces pombe
Apis mellifera
Tribolium castaneum
moths | 2 leaves
Acyrthosiphon pisum
flies | 3 leaves
bony fishes | 3 leaves
Xenopus laevis
synthetic construct
Macaca mulatta
Pan troglodytes
Macaca fascicularis
Canis lupus familiaris
Pan troglodytes
Homo sapiens
Bos taurus
Canis lupus familiaris
Equus caballus
Monodelphis domestica
sea urchins | 3 leaves
Nematostella vectensis
apicomplexans | 5 leaves
Plasmodium knowlesi strain H
Plasmodium vivax Sal-1
apicomplexans | 4 leaves
PfNapL
Plasmodium falciparum 3D7

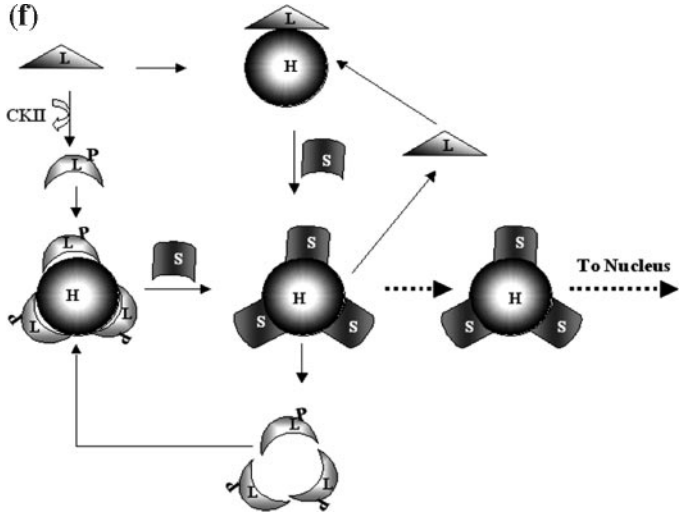

FIGURE 1—*continued*

Gene Knock-out Studies on PfNapL—To investigate whether the function of PfNapL could be disrupted, we designed a construct to specifically target the PfNapL gene and to replace it with an human dihydrofolate reductase-selectable marker cassette. Despite several attempts, we were not able to obtain a population where the PfNapL gene was replaced by the human dihydrofolate reductase cassette (Fig. S2). Although we cannot exclude any technical problems, the inability to disrupt the function of PfNapL is indicative of a pivotal role of this gene product for the survival of *P. falciparum*. At the moment, our repertoire of molecular tools in *P. falciparum* precludes us from performing conditional gene disruptions. An essential or at least a very beneficial role of this molecule has been described in several other organisms like mouse and *Drosophila* (9, 10). Therefore, we propose that the PfNapL protein is very likely to be essential for parasite survival and that it provides a potential new target for disruption of parasite nucleosome assembly as a route toward controlling parasite growth.

Structural Conservation with yNAP-1, hSET, and Vps75—The root mean square (r.m.s.) deviation derived from the least square fittings of 191 C^{α} of PfNapL with the corresponding C^{α} of yNAP-1, hSET, and Vps75 is 1.9, 1.8, and 1.8 Å, respectively (Fig. 2*a* and Fig. S3). The dimerization helix α2 of PfNapL shows an r.m.s. deviation of 1.4 and 1.1 Å with the corresponding dimerization helices of yNAP-1 and hSET (Fig. 2, *b* and *c*). The core domain II of PfNapL is also similar to yNAP-1 and hSET, with an average r.m.s. deviation of 1.1 and 1.0 Å, respectively (Fig. 2, *b* and *c*). The dimerization helix α2 of PfNapL has high sequence similarity with the corresponding dimerization helices of hSET/yNAP-1 for a total of ~50 residues (Fig. 2, *b* and *c*). In the β subdomain, PfNapL has 16 of 24 identical and 5 of 8 conserved residues with the corresponding β subdomains of hSET/yNAP-1. The residues 290–295 of this antiparallel β-sheet region of yNAP-1 had been previously identified as the nuclear localization signal (NLS) (15) (Figs. 1*c* and 2, *b* and *c*). Residues 200–221 in PfNapL corresponding to this short antiparallel β-sheet region (β5 and β6) in yNAP-1 are disordered (Fig. 2*b*). However, the NLS sequences between yeast and PfNapL are highly conserved (Figs. 1*c* and 2*b*).

PfNapL Lacks the "Accessory Domain" Conserved in Higher Eukaryotic NAPs—Comparison between yNAP-1, hSET, and PfNapL structures revealed that yNAP-1 contains an additional α-helix, termed the "accessory domain," which has been inserted between domain I and II but is absent in both hSET and PfNapL (Figs. 1*c* and 2*a*). Based on the sequence comparison, it can be inferred that this accessory domain is present in all other eukaryotic nucleosome assembly proteins but is seen to be specifically absent in PfNapL and other NAPs from *Plasmodium* species (Fig. 1*d*). Intriguingly, SET protein homologs, such as the recently characterized human SET (16), are absent in yeast and *Plasmodium* (stand alone SET domains are found in higher eukaryotes like mice, cows, and humans). In *Plasmodium*, SET-like domains are a constituent of significantly larger proteins (molecular mass ≥142 kDa) termed "SET domain proteins," where functions and localizations are still unknown (PFD0190w, PFF1440w, and PF08_0012).

PfNapL Dimer and Conserved Hydrophobic Motifs—The dimer formation in yNAP-1, hSET, Vps75, and PfNapL is achieved via the dimerization helix α2. In PfNapL, residues Gln^{50}, Glu^{52}, Tyr^{54}, Glu^{57}, Lys^{59}, Glu^{63}, Arg^{68}, Lys^{70}, Tyr^{71}, and Lys^{81} of the dimerization helix α2 and Pro^{271}, Tyr^{272}, and Asp^{275} of helix α8, which lies on the other side of the β subdomain contribute to dimer formation. Residues Glu^{52} and Glu^{63} and Lys^{70} and Lys^{81} of the dimerization helix α2 form salt bridges. The hydrogen bonding interactions contributing to dimer formation in PfNapL are mostly structurally conserved with those of hSET (Fig. 1*c*). Unlike yNAP-1, the PfNapL dimerization helices are bent at ~50° very similar to the hSET and Vps75 dimers (Fig. S4*a* and Fig. S5*a*). Although a proline residue at position 77 is present in PfNapL, there are no kinks formed in the dimerization helices upon dimer formation in PfNapL in contrast to yNAP-1 (Fig. S4*a*). Interestingly, PfNapL

FIGURE 1. **The overall structure of PfNapL.** *a*, domain diagram for the NAP/SET family of proteins. Histone chaperone proteins comprise a central domain and low complexity N and C termini. The inserted accessory domain in yNAP-1 (yellow) is highlighted, which is missing both in PfNapL and hSET (set to scale). The *brown bar* is not set to scale, since the N and C termini are variable. *b*, structure of the PfNapL dimer generated using 2-fold crystallographic symmetry operation. Each monomer of PfNapL contains a domain I composed of dimerization helix α2 and domain II composed of a β subdomain (four antiparallel β strands) and α-helices on the other side. *c*, structure-based sequence alignment of PfNapL, yNAP-1, and hSET. The structures share high structural homology, except for an additional accessory domain between domain I and domain II in yNAP-1 (*foreground colored yellow*). Residues contributing to dimer formation are *colored green*. Conserved hydrophobic motifs, predicted NES, and predicted NLS in PfNapL are *underlined* in *purple* and *blue*, respectively. Conserved residues from the hSET mutagenesis data are *colored red* and *blue*. *d*, sequence alignment of PfNapL and other eukaryotic members of the NAP family: yNAP-1 (*Saccharomyces cerevisiae*), xNAP-1 (*Xenopus laevis*), dNAP-1 (*Drosophila melanogaster*), and hNAP-1 (*Homo sapiens*). The accessory domain in yNAP-1 is *foreground-colored yellow*. The identical/conserved surface residues and conserved hydrophobic motifs are *colored pink* and *purple*, respectively. *e*, phylogenetic tree of NAPs from various species showing greater evolutionary distance of malaria parasite NAPs from homologs in yeast and humans (indicated by *red arrows*). *f*, model for *in vitro* relay of histones by *P. falciparum* nucleosome assembly proteins. This model was reproduced from Ref. 14, showing distinct roles for PfNapL (in cytoplasm as a histone carrier) and PfNapS (in nucleus capable of histone deposition). PfNapL (*L*) interacts with histones and can deliver histones to PfNapS (*S*; phosphorylated or unphosphorylated) readily. PfNapL upon phosphorylation (L^P) binds 3-fold better to the histones when compared with the unphosphorylated form of PfNapL. Phospho-PfNapL may deliver its histone cargo PfNapS. The latter takes over histones from Phospho-PfNapL-histone complexes and shuttles the histones into nucleus.

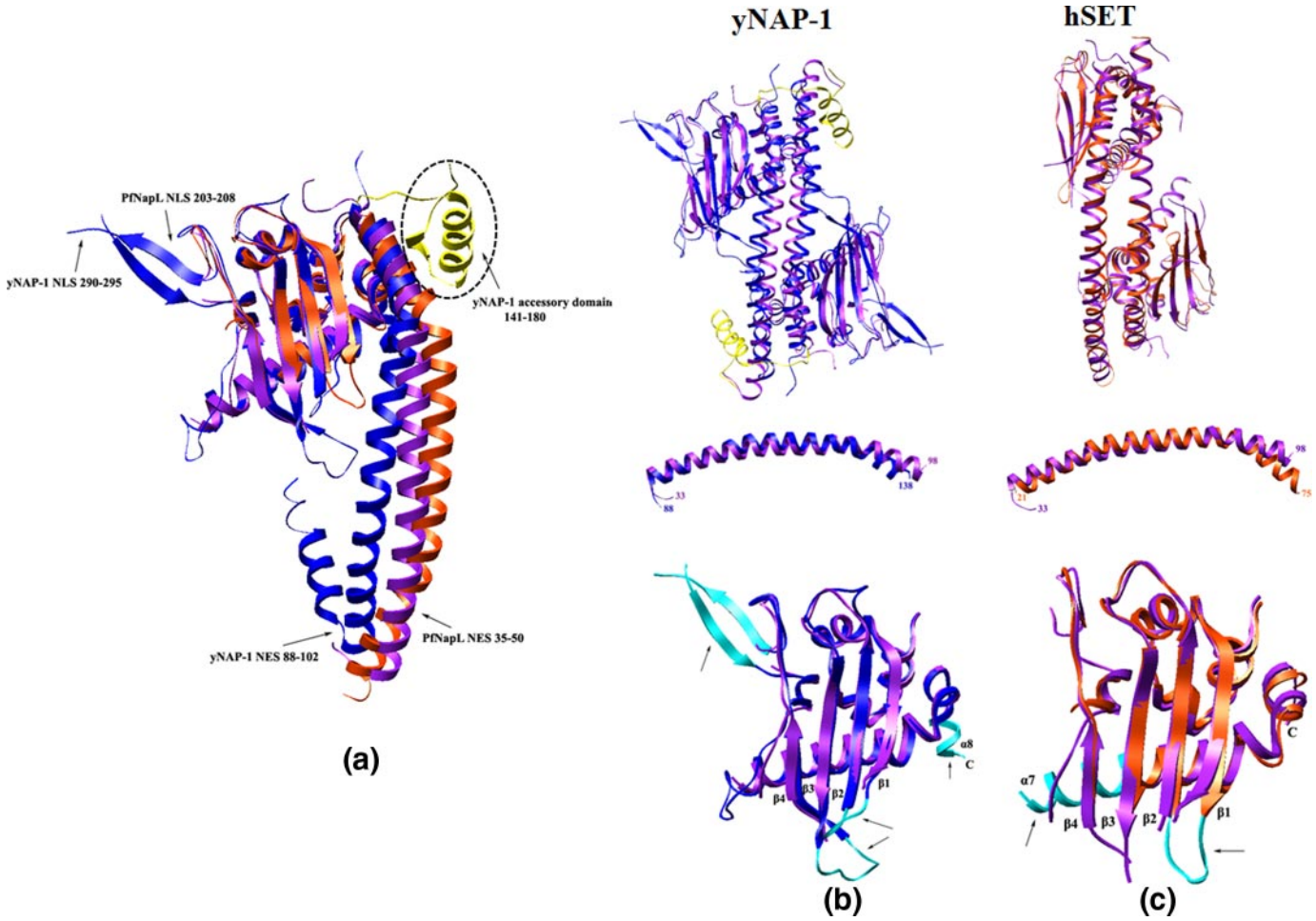

FIGURE 2. **Comparison of PfNapL structure with yNAP-1 (Protein Data Bank code 2AYU) and hSET (Protein Data Bank code 2E50).** *a*, superimposition of PfNapL monomer (*purple*) onto yNAP-1 (*blue*) and hSET (*orange*). Accessory domain of yNAP-1 is *colored yellow*. NES and NLS in yNAP-1 and PfNapL are indicated. *b*, superimposition of PfNapL and yNAP-1 dimers. The *lower half* shows superimposition of domain I and II from PfNapL and yNAP-1 monomers. yNAP-1 is *colored blue*, and the accessory domain is *colored yellow*. PfNapL is *colored purple*. The extra residues in domain II of yNAP-1 are *colored cyan* and are disordered in PfNapL. *c*, superimposition of PfNapL and hSET dimers. The *lower half* shows superimposition of domain I and II from PfNapL and hSET monomers. The extra residues of PfNapL are *colored cyan* and are disordered in hSET.

dimer displays a somewhat narrow cavity (Fig. S5*b*) when compared with Vps75 dimer (18, 19). In yNAP-1, a disulfide bond is formed by residues Cys^{249} and Cys^{272}. These positions are replaced by serine and threonine in PfNapL, and only a single cysteine is present in PfNapL at position 133. The hydrophobic core of PfNapL and yNAP-1 is stabilized by the presence of SFF(T/N)FF and (L/I)P(E/S)FWL motifs that are conserved among the NAP family (Fig. 1*c* and Fig. S4*b*).

PfNapL Localization in Parasite Cytoplasm Using Transfection Studies—We have earlier shown that PfNapL is expressed during all of the blood stages and is localized to the parasite cytoplasm (13, 14). PfNapL also contains conserved NLS and NES motifs (Figs. 1*c* and 3, *b* and *c*) like the yNAP-1 (which is observed in both the cytoplasm and the nucleus). Corresponding to the presence of NES in yNAP1 (residues 88–103) (Fig. 3*a*), residues 35–50 of PfNapL have been predicted as an NES (Fig. 3, *b* and *c*). It has been suggested in yNAP-1 that this NES is masked by the accessory domain, which is thought to play an important role in the import and export of yNAP-1 into and from the nucleus (15) (Fig. 3*a*). As mentioned earlier, this accessory domain in yNAP-1 (residues 141–180) is the inserted α-helix, which is absent in PfNapL (Figs. 1*c* and 2*a*). Interestingly, hSET also lacks this accessory domain yet contains both NES and NLS motifs (16). Further, hSET is localized both in the cell cytoplasm and the nucleus, similar to yNAP-1 (36) and like other histone shuttling proteins. In this respect, PfNapL clearly stands as an exception despite its structural and sequence similarities with yeast NAP and human SET proteins.

In order to address whether PfNapL is located at some stage in the nucleus and whether its cytosolic localization is due to continuous export mediated by its putative NES, we generated cell lines expressing PfNapL-GFP chimeras. For these chimeras, we either used wild-type sequence or introduced mutations in the conserved residues of the NES (PfNapL L46A or PfNapL Q50A) (Fig. 3*c*). Disruption of a functional NES was predicted to lead to the accumulation of GFP chimera in the parasite nucleus. Expression of the GFP chimeras was verified via Western blot and probed with anti-GFP antibodies (Fig. 4*a*). A band of ~70 kDa was observed in all cell lines, corresponding to the size of PfNapL (40.5 kDa) fused to GFP (26.8 kDa). The GFP fusion protein of all three transfectants (wild type and mutants) was detectable in the cytoplasm of all stages. Previous localiza-

tion experiments with PfNapL-specific antibodies detected an exclusive cytoplasmic localization in all stages, except for the schizont stages, where the separation between nuclear (DAPI) and PfNapL staining was less defined (13). This could be due to greater interdigitation of the nucleus and cytoplasm at that stage or due to a closer association of the PfNapL pool with the nucleus. To address this question, we followed the localization of PfNapL wild type over the asexual erythrocytic life cycle (Fig. 4, *b–d*). PfNapL wild type-GFP was detected in the cytoplasm of the parasites. No fluorescence could be detected in the erythrocyte cytosol. Neither the food vacuole nor the nucleus of the parasite showed fluorescence in any parasite stage. This indicates that PfNapL is exclusively located in the cytoplasm of the parasite and that its putative NES is not necessary for its localization, and the predicted NES is not functional/relevant in PfNapL.

The Electrostatic Potential of PfNapL Dimer—Analysis of the electrostatic potential of PfNapL dimer indicates that the convex region of the dimerization helix $\alpha 2$ has acidic residues scattered on the surface in an alternate manner (Glu^{38}, Glu^{41}, Glu^{52}, Asp^{55}, Glu^{63}, Asp^{80}, and Glu^{84}) (Fig. 5). There are also three basic residues toward the end of this helix (Lys^{70}, Lys^{81}, and Arg^{82}) contributing to a slightly basic nature and hence an uneven charge distribution (Fig. 5). The domain II of PfNapL dimer has a hydrophobic nature on one side and is highly negatively charged on the opposite face with several residues (Glu^{119}, Glu^{122}, Glu^{123}, Glu^{252}, Glu^{256}, Asp^{258}, Glu^{260}, and Glu^{267}), forming a cavity that is also a characteristic feature of the yNAP-1 and hSET (Fig. 5). The bottom of this cavity has an uneven charge character, and a single acidic residue, Glu^{61}, is present at its base. It has been previously suggested for yNAP-1 that this highly acidic cavity might be important for binding to basic histones (15). The residues Asp^{119}, Glu^{122}, Glu^{123}, Asp^{258}, Glu^{260}, and Glu^{267} that constitute this cavity in PfNapL are structurally conserved with yNAP-1 and hSET, hence highlighting their possible significance.

Prediction of Essential Residues Involved in Histone Binding by PfNapL—Most histone chaperones contain long acidic stretches in their C-terminal region, which were thought to be involved in histone

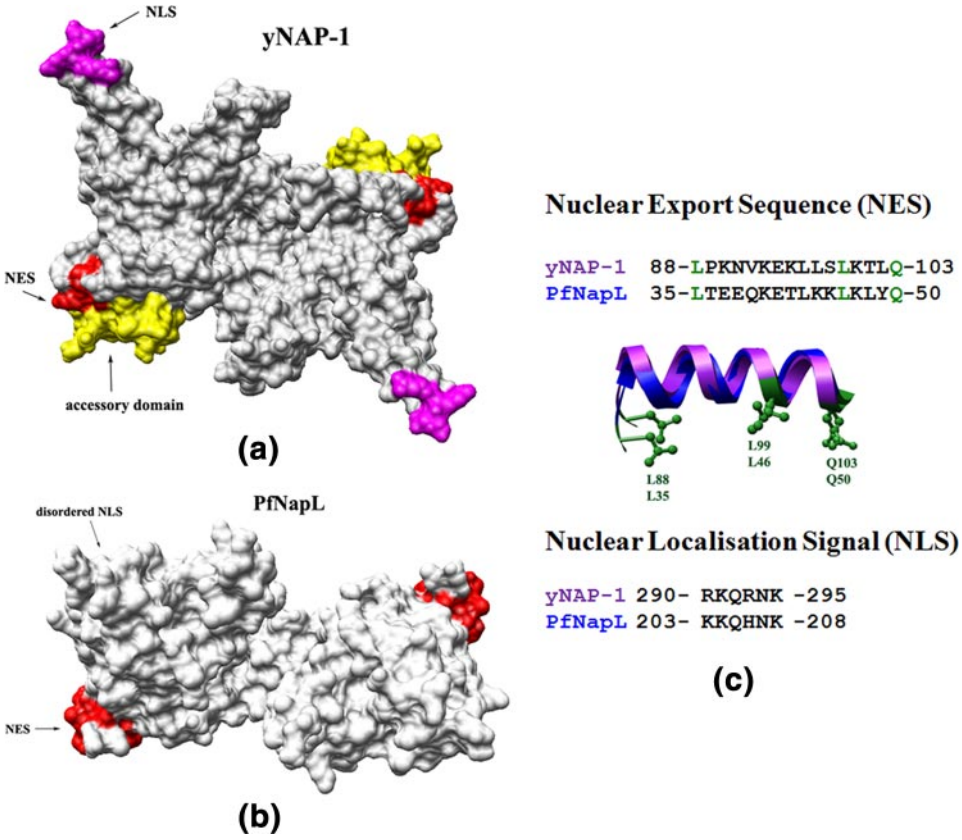

FIGURE 3. **NES and NLS motifs in yNAP-1 and PfNapL.** *a*, surface representation of yNAP-1. NES, accessory domain, and NLS are *colored red*, *yellow*, and *magenta*, respectively. *b*, surface representation of PfNapL. Predicted NES is colored *red*. The predicted NLS is indicated. *c*, sequence alignment of NES and NLS in yNAP-1 and PfNapL. The key residues are *colored green*. Superimposition of NES in yNAP-1 and PfNapL is shown with key residues shown in *green* as *ball-and-stick representations*.

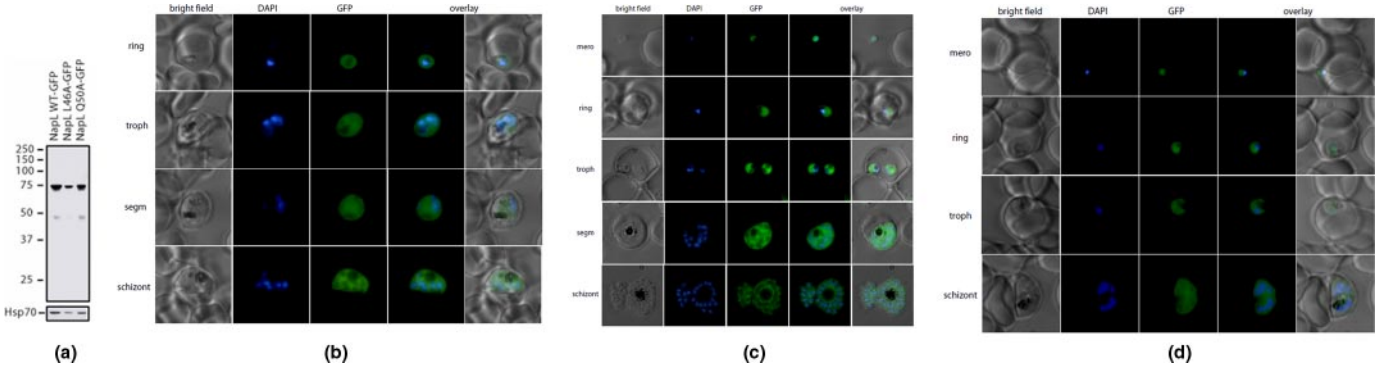

FIGURE 4. **Stage specific expression of PfNapL-GFP chimeras.** *a*, Western blot of transgenic cell lines expressing GFP-tagged versions of NapL with antibodies against GFP. Expression of PfHsp70 was detected to ensure similar loading. The localization of PfNapL wild type-GFP (*b*), PfNapL L46A-GFP (*c*), and PfNapL Q50A (*d*) in different stages of the erythrocytic life cycle of *P. falciparum* is shown. The *first column* of each *panel* shows bright field pictures, followed by a nuclear DAPI stain, GFP fluorescence, an overlay of the nuclear and GFP localization, and (in the *last column*) overlay of bright field with DAPI and GFP.

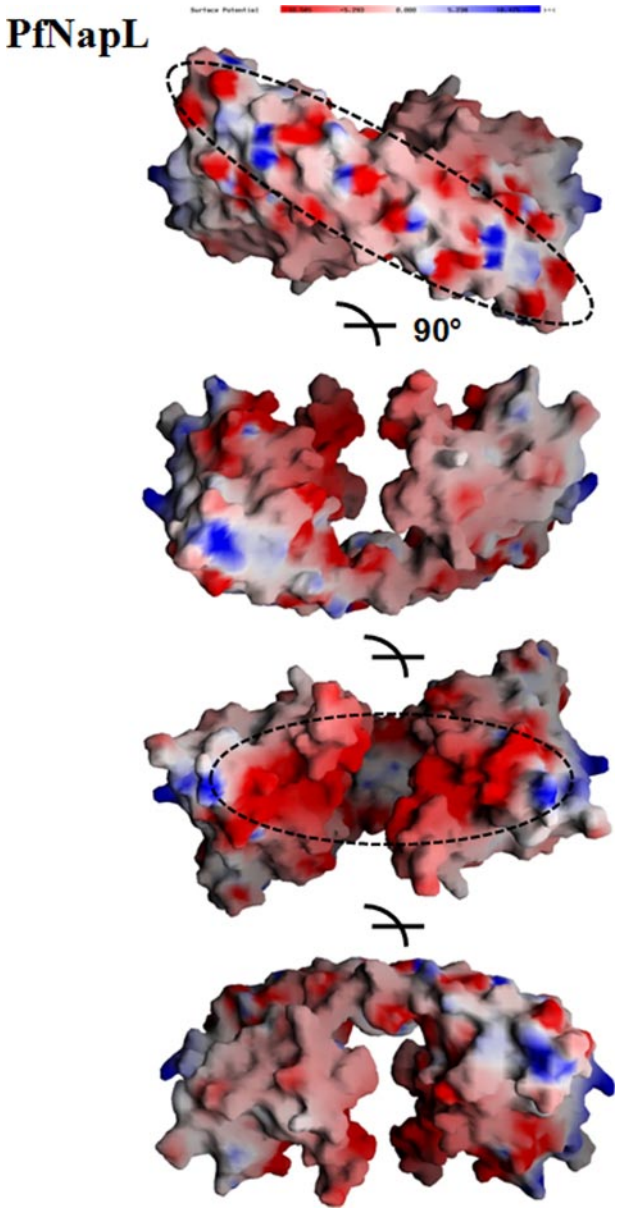

FIGURE 5. **Electrostatic potential distribution of the PfNapL dimer.** The convex region of the dimerization helix α2 contains acidic residues scattered on the surface in an alternate manner. Domain II of PfNapL forms a cavity consisting of mostly acidic residues that are conserved with yNAP-1 and hSET.

binding, considering the highly basic character of histones. However, recent studies have shown that these acidic stretches are not essential for histone binding activities for chaperones yNAP-1, Asf1, nucleoplasmin, etc. (5, 15, 37). It is noted that full-length PfNapL also has an acidic stretch of residues in its C-terminal region similar to yNAP-1 and hSET, with an average pI of ~3.0 calculated using amino acid sequence (Fig. 1*a*). Mutagenesis studies on hSET revealed important residues of domain II that affect the binding of hSET to both core histones and double-stranded DNA (16). We have mapped these residues on yNAP-1 and PfNapL (Fig. 6*a*). Based upon these hSET mutagenesis data, we identified several corresponding residues in PfNapL and mutated them to test their relevance in histone recognition. We constructed six single-site mutants of the corresponding residues from PfNapL (D192A, H227A, T230A, Y259A, E260A, and K266A). In addition, we made one other mutant (D223A) that is conserved, exposed, and proximal to the previously implicated histone recognition residues from hSET (16). Our PfNapL-histone binding data, using purified proteins of high quality, show that none of these seven mutations altered histone binding of PfNapL to histones H3, H4, H2A, or H2B, to histone tetramer, or to histone octamer significantly (Fig. 6*b*). We therefore propose that it is likely for histones to have different a binding site(s) on PfNapL (and possibly on other NAPs) in comparison with hSET-histone interactions (16). These residues are not identical among PfNapL, hSET, yNAP-1, and Vps75 proteins, and in general, residues proposed by hSET-histone studies show weak conservation (Table S1). An overall structure-based residue comparison between yNAP-1, Vps75, hSET, and PfNapL reveals very few regions of sequence conservation (Fig. S1). In order to further probe the potential sites for histone recognition by PfNapL, we inspected the surface residues of PfNapL (keeping in view structure and sequence information from NAPs). Here, we have highlighted the identical/conserved surface residues in the NAP family (Figs. 1*d* and 7) based on the described criterion.

Comparisons with Asf1-Histone Complex—The β subdomain of PfNapL is a highly conserved feature of NAPs and is also found in other histone chaperones like Asf1 (20). The crystal structure of the human Asf1 has been recently determined in complex with H3-H4 dimer, highlighting the crucial residues involved in histone binding (20, 21). A structural comparison of the four-stranded β subdomain of PfNapL with Asf1 shows a superimposition with an r.m.s. deviation of 0.97 Å (Fig. 8*a*). Further, there are no steric hindrances between the overall PfNapL dimer and H3-H4 dimer (Fig. S6). Mapping of the interacting residues as highlighted for human Asf1 revealed three corresponding, structurally conserved surface residues in PfNapL (Ile^{136}, Ile^{147}, and Ala^{185}) (Fig. 8*b*). Further, three residues of PfNapL are conserved among the NAP family (Fig. 8*c*) and may represent common sites for histone recognition. Based on structural congruence, we propose that these residues in PfNapL may interact with Leu^{126} and Ile^{130} of H3 and Thr^{96} and Leu^{97} of histone H4. To validate the above modeling, we mutated the putative interacting PfNapL residues, Ile^{136} and Ile^{147}, to alanines and tested the mutant proteins for H3-H4 tetramer binding ability. Our protein-protein-based ELISA data indicate a significant (up to two-thirds) reduction in binding between PfNapL and H3-H4 tetramer (Fig. 8*d*).

DISCUSSION

The structure of PfNapL was determined using the iodide-SAD technique and refined to 2.3 Å resolution. Structural analysis of PfNapL has revealed that PfNapL conforms to the domain architecture of nucleosome assembly proteins, exhibiting a high complexity ordered central region and largely disordered N- and C-terminal regions. PfNapL forms a homodimer that acquires a fold similar to the yNAP-1, hSET, and Vps75 dimers (15–17). These investigations demonstrate high structural homology within these proteins despite a low level of sequence identity (only 14–25%) (Fig. 1*c*). The major difference between PfNapL and yNAP-1 lies in the absence of

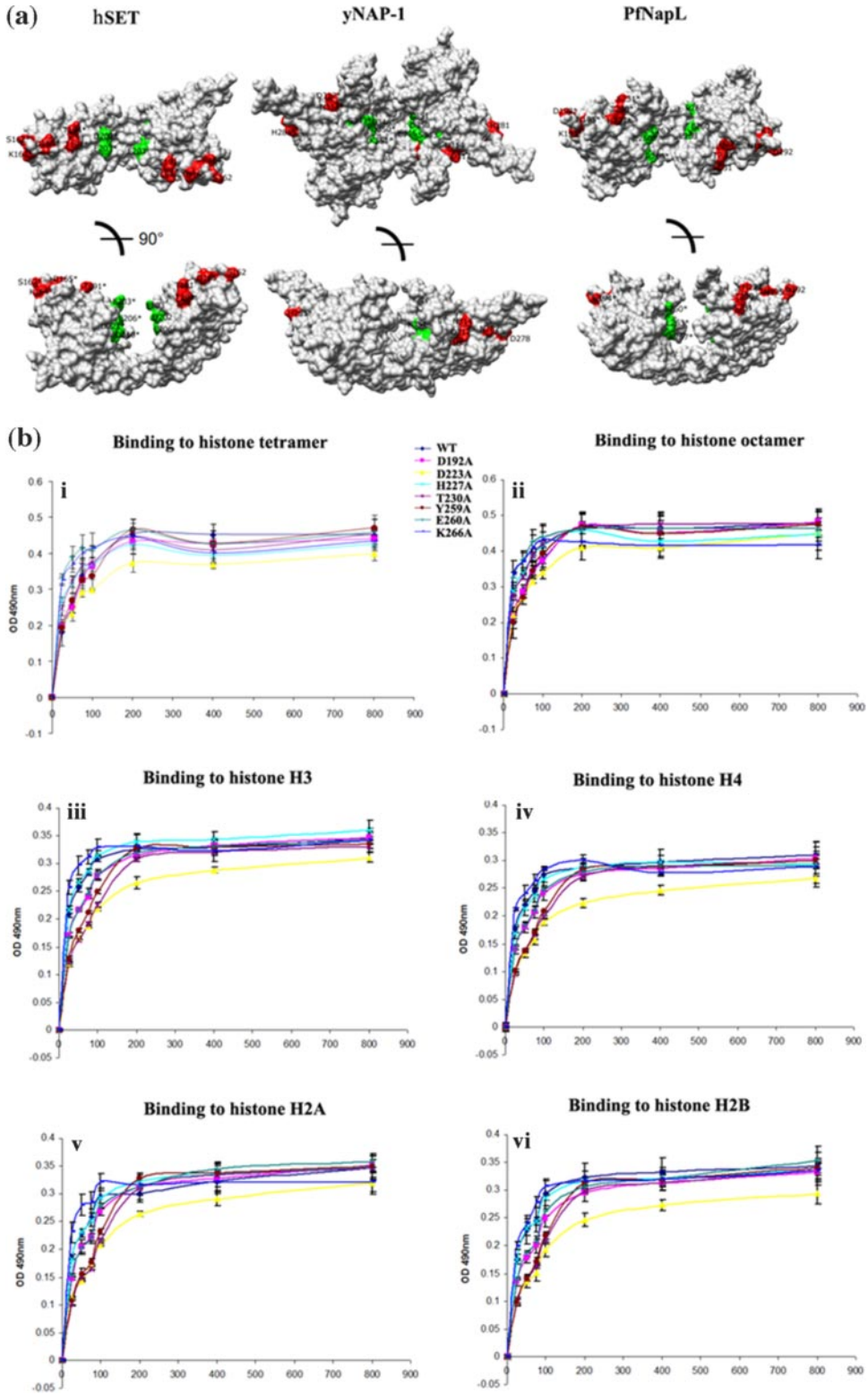

FIGURE 6. *a*, orthogonal views of the surface representation of hSET, yNAP-1, and PfNapL dimers with important residues from the mutagenesis data of hSET *colored green* and *red*. *b*, histone-binding activities of PfNapL wild type and mutants (D192A, H227A, T230A, E260A, K266A, D233A, and Y259A). Shown is binding with histone tetramer (*i*), histone octamer (*ii*), H3 (*iii*), H4 (*iv*), H2A (*v*), and H2B (*vi*).

the accessory domain in PfNapL that is inserted between the dimerization helix α2 and domain II in yNAP-1 (15) (Fig. 1*d*). Phylogenetic analysis of NAPs suggests greater evolutionary distance of PfNapL from homologs in higher eukaryotes (Fig. 1*e*), although malaria parasite NAPs are unique in their lack of the accessory domain. We have earlier shown that PfNapL is a unique, nonredundant protein in *P. falciparum*, and it performs an exclusive role in the nucleosome assembly activity in the parasite (13, 14). Previous studies on gene knock-out phenotypes in several organisms like mouse and *Drosophila* have indicated the essentiality of the NAP family (9, 10). Furthermore, our inability to disrupt the gene for PfNapL corroborates the essentiality of this protein in *P. falciparum* (Fig. S2).

Corresponding to yNAP-1, PfNapL also contains NES and NLS motifs (Figs. 1*c* and 3*c*). We have previously shown that PfNapL is predominantly localized to the cytoplasm and is centrally responsible for shuttling and transfer of histones to PfNapS (which is localized to both cytoplasm and the nucleus and which eventually deposits histones onto DNA). PfNapL and PfNapS do not interact with each other (14). Therefore, PfNapL is principally localized to the cytoplasm and does not possess the ability to deposit the histones in the nucleus (14). In this context, it is interesting to note that hSET also lacks the accessory domain of yNAP-1/other NAPs, but unlike PfNapL, hSET is localized both in cytoplasm and the nucleus (22). Since this accessory domain is absent in PfNapL (Fig. 2*b*), the predicted NES on the PfNapL structure is thus exposed and not be masked by the accessory domain, as suggested and observed for yNAP-1 (15) (Fig. 3, *a* and *b*). From a structural perspective, this further validates the localization of PfNapL to the cytoplasm. The histone binding characteristics of PfNapL have been detailed previously, including its ability to transfer cytoplasmic histones on to PfNapS. A model for relay of histones from parasite cytoplasm to the nucleus has also been proposed by us previously (see Ref. 14 and specifically Fig. 1*f* reproduced here from Ref. 14). Our published reports on the two *Plasmodium* parasite nucleosome assembly proteins have clearly suggested different

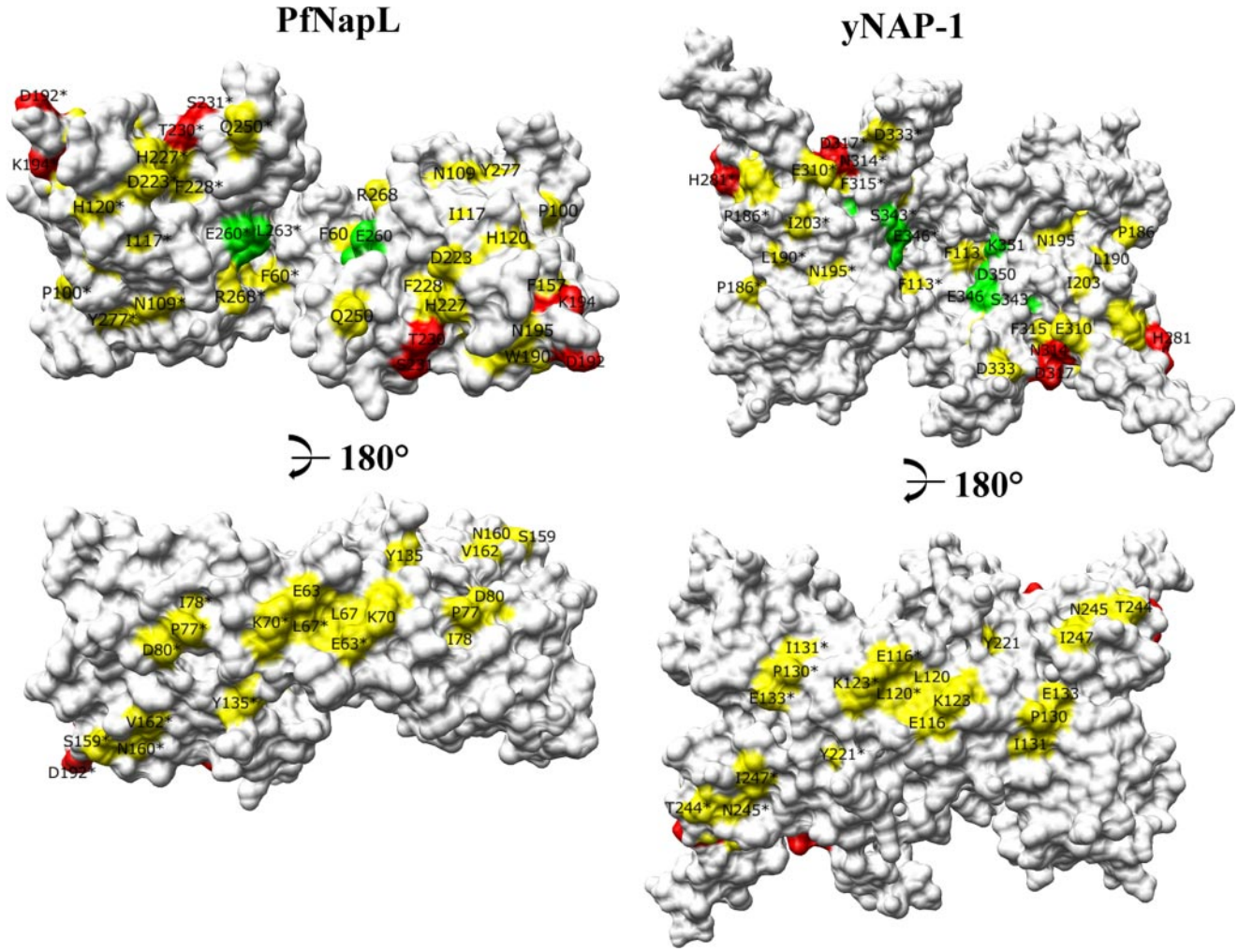

FIGURE 7. **Two views of the surface representation of PfNapL and yNAP-1 dimers.** Corresponding residues from the mutagenesis data of hSET are *colored green* and *red*. The identical/conserved surface residues within the NAP family are *colored yellow*.

roles for PfNapL (in histone shuttling in the cytoplasm) and for PfNapS (which is localized both in the cytoplasm and nucleus and which can perform histone deposition onto DNA (13, 14) (Fig. 1*f*).

Electrostatic potential distribution of PfNapL dimer reveals a stretch of alternate acidic residues on the convex surface of the dimerization helix α2 and a highly acidic side to domain II. If this convex surface of the PfNapL dimer is implicated in histone recognition, then it can be suggested that the highlighted acidic residues on this surface might be making alternate contacts with an α-helix of a core histone (Fig. 5). In yNAP-1, the acidic stretch forming a cavity in domain II has been shown to be involved in neutralizing and binding the basic N-terminal histone tails (15). Also, most of the acidic residues constituting this cavity are structurally conserved among PfNapL and yNAP-1. Thus, based upon the earlier suggestions for yNAP-1, this acidic region in PfNapL may be involved in histone recognition (Fig. 5).

Mapping of the corresponding residues from hSET mutagenesis data onto PfNapL and yNAP-1 demonstrates the conserved nature of 10 of these residues among PfNapL, hSET, and yNAP-1 (Fig. 6*a*). However, mutation of some of these residues on PfNapL did not significantly alter PfNapL-histone binding (Fig. 6*b*). Consequently, based upon our mutagenesis data analysis, we suggest that the binding site(s) and/or essential residues for the recognition of core histones may be different for PfNapL from those proposed by hSET-histone interactions (16). A structure-based comparison of the residues that were mutated in PfNapL reveals that none of these are identical among hSET, yNAP-1, Vps75, and PfNapL. Indeed, only a few show weak conservation (Table S1). Also, an overall structure-based comparison between yNAP-1, Vps75, hSET, and PfNapL reveals very few regions of sequence conservation (Fig. S1). These observations therefore suggest that histone recognition site(s) for hSET may not be applicable for nucleosome assembly proteins like PfNapL and yNAP-1. Our mapping of highly conserved and surface-exposed residues in the NAP family provides some clues for the possible set of essential residues that might underpin NAP-histone binding (Figs. 1*d* and 7). Several of these conserved residues lie in and around the characteristic cavity formed by the PfNapL dimer, which has been previously implicated in histone recognition in both yNAP-1 and hSET (15, 16). Distribution of these conserved surface residues on the convex region of PfNapL dimer illustrates their proximity to and overlap with the alternate stretch of acidic residues highlighted by our electrostatic potential analysis.

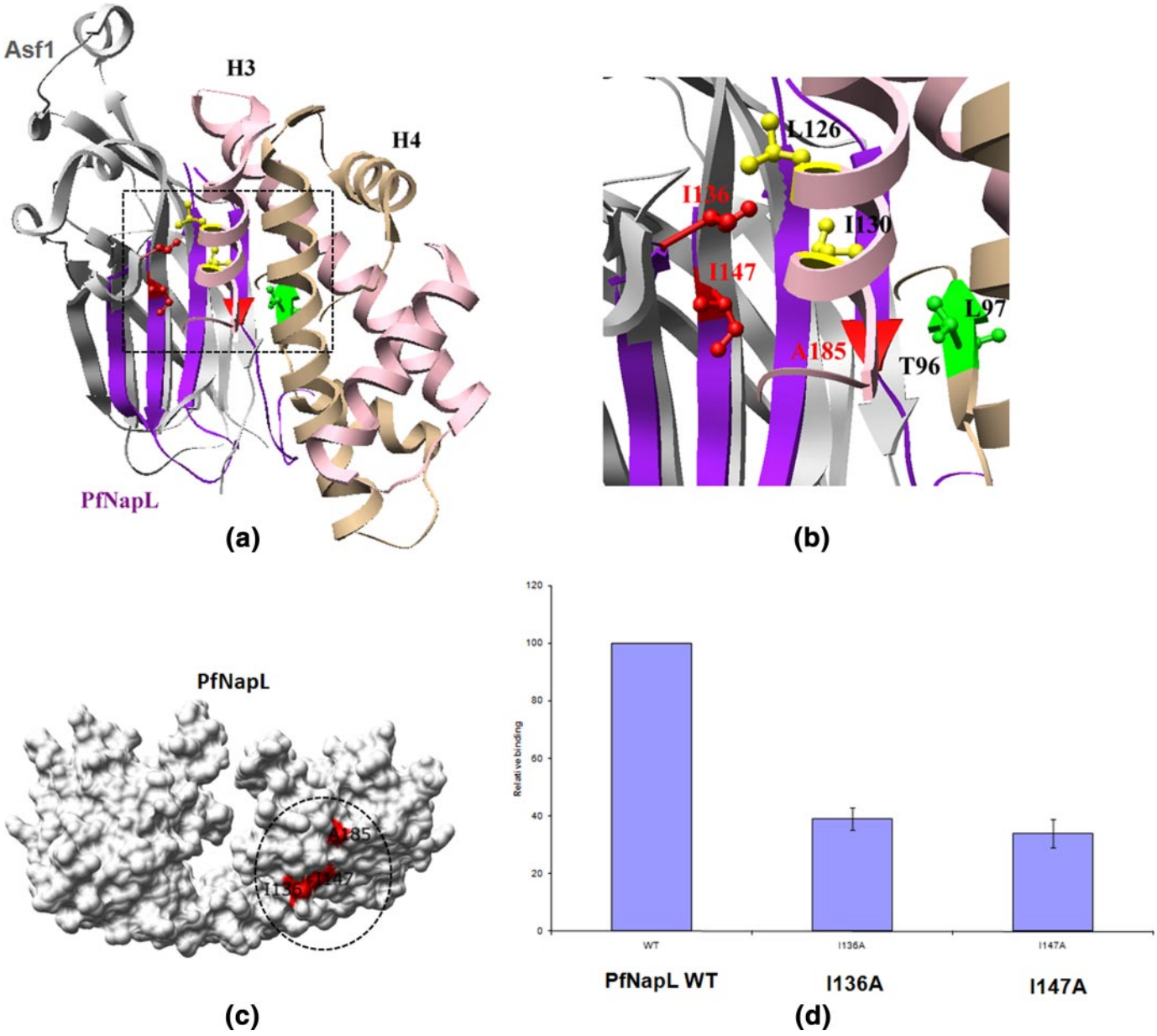

FIGURE 8. **Comparison of PfNapL dimer with the Asf1-histone complex (Protein Data Bank code 2HUE).** *a*, superimposition of the β subdomain of PfNapL (*purple ribbon*) and Asf1-histone complex wherein Asf1, H3, and H4 are *colored light gray*, *pink*, and *brown*, respectively. The conserved residues of PfNapL are shown in a *red ball-and-stick representation*. The interacting residues of H3 and H4 are shown in a *yellow* and *green ball-and-stick representation*. *b*, close view of the proposed interaction. *c*, surface representation of PfNapL with predicted histone-binding residues *colored red*. *d*, histone-binding activity of PfNapL wild type and mutants (I136A and I147A) with H3-H4 tetramer.

It is known that the β subdomain present in yNAP-1, hSET, and PfNapL is a highly conserved feature of histone chaperones (Fig. 2*a*). The superimposition of the β subdomain of PfNapL onto histone chaperone Asf1 revealed three conserved surface residues on PfNapL (conserved in all NAPs) that are suggested to be important for interaction with H3-H4 dimer based upon the Asf1 and H3-H4 dimer interactions (21) (Fig. 8, *a*–*d*, and Fig. S6). Interestingly, the three residues identified in Asf-histone complex map to a region of PfNapL that is not implicated by either hSET mutagenesis or by our mapping of conserved, exposed residues in NAPs. This suggests that Asf1 and NAPs may recognize histones differently. Further, modeling of PfNapL based on the Asf1-histone complex crystal structure clearly suggests three target residues that are likely to participate in H3-H4 recognition. Based on these structural insights, we mutated two of the three residues (the third one is an alanine in any case) and confirmed the idea that their alteration to alanine reduces binding of PfNapL to H3-H4 tetramer significantly (Fig. 8*d*).

In summary, our studies provide further structural insights into histone chaperones from *P. falciparum* and highlight key regions of differences between plasmodial NAPs and their counterparts. Although further dissection of the modes of histone recognition by NAPs will be required to gain a complete understanding of the mechanism of histone binding and transport by nucleosome assembly proteins, it is already clear that the parasite NAPs are sufficiently different from their counterparts in other species. Our genetic-structural-functional data

on PfNapL suggests PfNapL as a possible new focus for development of antimalarials.

Acknowledgment—We thank Prof. Alan Cowman for support and for the generous gift of reagents.

REFERENCES

1. Luger, K., Maeder, A. W., Richmond, R. K., Sargent, D. F., and Richmond, T. J. (1997) *Nature* **389,** 251–259
2. Krude, T. (1999) *Eur. J. Biochem.* **263,** 1–5
3. Eitoku, M., Sato, L., Senda, T., and Horikoshi, M. (2008) *Cell. Mol. Life. Sci.* **65,** 414–444
4. Park, Y., Chodaparambil, J. V., Bao, Y., McBryant, S. J., and Luger, K. (2005) *J. Biol. Chem.* **280,** 1817–1825
5. Dutta, S., Akey, I. V., Dingwall, C., Hartman, K. L., Laue, T., Nolte, R. T., Head, J. F., and Akey, C. W. (2001) *Mol. Cell.* **8,** 841–853
6. Jackson, V., Shires, A., Tanphaichitr, N., and Chalkley, R. (1976) *J. Mol. Biol.* **104,** 471–483
7. Annunziato, A. T., and Seale, R. L. (1983) *Mol. Cell. Biochem.* **55,** 99–112
8. Koning, L. D., Corpet, A., Haber, J. E., and Almouzni, G. (2007) *Nat. Struct. Mol. Biol.* **14,** 997–1007
9. Rodriguez, P., Munroe, D., Prawitt, D., Chu, L. L., Bric, E., Kim, J., Reid, L. H., Davies, C., Nakagama, H., Loebbert, R., Winterpacht, A., Petruzzi, M., Higgins, M. J., Nowak, N., Evans, G., Shows, T., Weissman, B. E., Zabel, B., Housman, D. E., and Pelletier, J. (1997) *Genomics* **44,** 253–265
10. Lankenau, S., Barnickel, T., Marhold, J., Lyko, F., Mechler, B. M., and Lankenau, D. (2003) *Genetics* **163,** 611–623
11. Tyler, J. K., Adams, C. R., Chen, S. R., Kobayashi, R., Kamakaka, R. T., and Kadonaga, J. T. (1999) *Nature* **402,** 555–560
12. Snow, R. W., Guerra, C. A., Abdisalan, M. N., Hla, Y. M., and Simon, I. H. (2005) *Nature* **434,** 214–217
13. Chandra, B. R., Olivieri, A., Silvestrini, F., Alano, P., and Sharma, A. (2005) *Mol. Biochem. Parasitol.* **142,** 237–247
14. Navadgi, M. V., Chandra, B. R., Mishra, P. C., and Sharma, A. (2006) *J. Biol. Chem.* **281,** 16978–16984
15. Park, Y.-J., and Luger, K. (2006) *Proc. Natl. Acad. Sci. U. S. A.* **103,** 1248–1253
16. Muto, S., Senda, M., Akai, Y., Sato, L., Suzuki, T., Nagai, R., Senda, T., and Horikoshi, M. (2007) *Proc. Natl. Acad. Sci. U. S. A.* **104,** 4285–4290
17. Selth, L., and Svejstrup, J. Q. (2007) *J. Biol. Chem.* **282,** 12358–12362
18. Tang, Y., Meeth, K., Jiang, E., Luo, C., and Marmorstein, R. (2008) *Proc. Natl. Acad. Sci. U. S. A.* **105,** 12206–12211
19. Berndsen, C. E., Tsubota, T., Lindner, S. E., Lee, S., Holton, J. M., Kaufman, P. D., Keck, J. L., and Denu, J. M. (2008) *Nat. Struct. Mol. Biol.* **15,** 948–956
20. English, C. M., Adkins, M. W., Carson, J. J., Churchill, M. E., and Tyler, J. K. (2006) *Cell* **127,** 458–460
21. Natsume, R., Eitoku, M., Akai, Y., Sano, N., Horikoshi, M., and Senda, T. (2007) *Nature* **446,** 338–341
22. Otwinowski, Z., and Minor, W. (1997) *Methods Enzymol.* **276,** 307–326
23. Adams, P. D., Grosse-Kunstleve, R. W., Hung, L. W., Ioerger, T. R., McCoy, A. J., Moriarty, N. W., Read, R. J., Sacchettini, J. C., Sauter, N. K., and Terwilliger, T. C. (2002) *Acta Crystallogr. Sect. D* **58,** 1948–1954
24. Emsley, P., and Cowtan, K. (2004) *Acta Crystallogr. Sect. D* **60,** 2126–2132
25. Brunger, A. T., Adams, P. D., Clore, G. M., Gros, P., Grosse-Kunstleve, R. W., Kuszewski, J.-S., Jiang, J., Nilges, N., Pannu, N. S., Read, R. J., Rice, L. M., Simonson, T., and Warren, G. L. (1998) *Acta Crystallogr. Sect. D* **54,** 905–921
26. Laskowski, R. A., MacArthur, M. W., Moss, D. S., and Thornton, J. M. (1993) *J. Appl. Crystallogr.* **26,** 283–291
27. Pettersen, E. F., Goddard, T. D., Huang, C. C., Couch, G. S., Greenblatt, D. M., Meng, E. C., and Ferrin, T. E. (2004) *J. Comp. Chem.* **25,** 1605–1612
28. Kleywegt, G. J. (1996) *Acta Crystallogr. Sect. D* **52,** 842–857
29. Nicholls, A., Sharp, K. A., and Honig, B. (1991) *Proteins Struct. Funct. Genet.* **11,** 281–296
30. Trager, W., and Jensen, J. B. (1978) *Nature* **273,** 621–622
31. Maier, A. G., Rug, M., Brown, M. T., O'Neill, M., Chakravorty, S., Szestak, T., Chesson, J., Wu, Y., Hughes, K., Coppel, R., Newbold, C., Beeson, J., Craig, A., Crabb, B. S., and Cowman, A. F. (2008) *Cell* **134,** 48–61
32. Crabb, B. S., Rug, M., Gilberger, T., Thompson, J. K., Triglia, T., Maier, A. G., and Cowman, A. F. (2004) *Methods Mol. Biol.* **270,** 263–276
33. Fidock, D. A., and Wellems, T. E. (1997) *Proc. Natl. Acad. Sci. U. S. A.* **94,** 10931–10936
34. Rug, M., Prescott, S. W., Fernandez, K. M., Cooke, B. M., and Cowman, A. F. (2006) *Blood* **108,** 370–378
35. Tanaka, Y., Tawaramoto-Sasanuma, M., Kawaguchi, S., Ohta, T., Yoda, K., Kurumizaka, H., and Yokoyama, S. (2004) *Methods* (*San Diego*) **33,** 3–11
36. Nagata, K., Saito, S., Okuwaki, M., Kawase, H., Furuya, A., Kusano, A., Hanai, N., Okuda, A., and Kikuchi, A. (1998) *Exp. Cell Res.* **240,** 274–281
37. Daganzo, S. M., Erzberger, J. P., Lam, W. M., Skordalakes, E., Zhangm, R., Franco, A. A., Brill, S. J., Adams, P. D., Berger, J. M., and Kaufman, P. D. (2003) *Curr. Biol.* **13,** 2148–2158